

NP-11-0035
August 4, 2011

10 CFR 52, Subpart A

U.S. Nuclear Regulatory Commission
ATTN: Document Control Desk
Washington, DC 20555-0001

Subject: Exelon Nuclear Texas Holdings, LLC
Victoria County Station Early Site Permit Application
Response to Request for Additional Information Letter No. 09
NRC Docket No. 52-042

Attached are responses to NRC staff questions included in Request for Additional Information (RAI) Letter No. 09, dated May 6, 2011, related to Early Site Permit Application (ESPA), Part 2, Sections 02.05.01 and 02.05.03. NRC RAI Letter No. 09 contained twenty-three (23) Questions. This submittal comprises the final partial response to RAI Letter No. 09, and includes response to the following two (2) Questions:

02.05.01-5
02.05.01-12

When a change to the ESPA is indicated by a Question response, the change will be incorporated into the next routine revision of the ESPA, planned for no later than March 31, 2012.

Of the remaining twenty-one (21) RAIs associated with RAI Letter No. 09, responses to six (6) Questions were submitted to the NRC in Exelon Letter NP-11-0022, dated June 2, 2011, responses to six (6) Questions were submitted to the NRC in Exelon Letter NP-11-0024, dated June 16, 2011, responses to eight (8) Questions were submitted to the NRC in Exelon Letter NP-11-0027, dated June 28, 2011, and response to one (1) Question was submitted to the NRC in Exelon Letter NP-11-0033, dated July 19, 2011. This submittal completes the Exelon response to NRC RAI Letter No. 09, dated May 6, 2011.

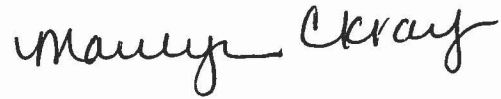
Regulatory commitments established in this submittal are identified in Attachment 3.

If any additional information is needed, please contact David J. Distel at (610) 765-5517.

August 4, 2011
U.S. Nuclear Regulatory Commission
Page 2

I declare under penalty of perjury that the foregoing is true and correct. Executed on the 4th day of August, 2011.

Respectfully,

A handwritten signature in black ink, appearing to read "Marilyn C. Kray". The signature is written in a cursive, flowing style.

Marilyn C. Kray
Vice President, Nuclear Project Development

Attachments:

1. Question 02.05.01-5
2. Question 02.05.01-12
3. Summary of Regulatory Commitments

cc: USNRC, Director, Office of New Reactors/NRLPO (w/Attachments)
USNRC, Project Manager, VCS, Division of New Reactor Licensing (w/Attachments)
USNRC Region IV, Regional Administrator (w/Attachments)

RAI 02.05.01-5:**Question:**

In SSAR Section 2.5 there are several cross-sections of shallow subsurface borehole data: Figures 2.5.1-34 and 35, and 2.5.4- 14, -15, and -16. For example, Fig. 2.5.4-14 shows a gentle step in topography and apparent offset of the Sand 1 / Clay 1-B contact between boreholes B-2302A and B-2308, which straddle the mapped trace of fault D.

- a. In support of 10 CFR 100.23(d)(2), and in order for the staff to evaluate the shallow subsurface units with respect to the presence (or lack thereof) of the fault, please develop cross-sections orthogonal to the trace of the fault and reevaluate the data to determine if there is an indication of a fault in the shallow subsurface.

Please add the following on all cross-section figures: stratigraphic or lithologic contacts (e.g. as shown in Figure 2.5.1-34); surface topography based on LiDAR; location of caliche layers; and location of fault(s). Also provide an explanation of the lithologic strip log.

- b. In SSAR Section 2.5.1.2.3, you stated that caliche intervals (SSAR Fig. 2.5.1-34 and 35) represent a series of paleosols and that could provide time stratigraphic markers. The staff notes that the paleosols may be more homogeneous and laterally continuous than the morphostratigraphic Beaumont Formation. Please explain why the paleosols were not used as a time-stratigraphic point for assessing the location and the timing of movement on fault D. Please provide descriptions of the calcic soils in all cross sections, such as thickness and stage of carbonate development (e.g. Birkeland, 1999, Soils and Geomorphology, Oxford Univ. Press). Also determine, based on depth measurements to the paleosol horizons across fault D, if any subtle deformation patterns indicate potential off-set on a fault plane.

Response:

The response to RAI 02.05.01-5 is organized to address the revision of two existing cross sections, X-X' and Y-Y', presented in SSAR Figures 2.5.1-34 and 2.5.1-35, and the development of two additional cross sections, W-W' and Z-Z', drawn orthogonal to the projection of growth fault D and its interpreted envelope of deformation. The cross sections and profiles and an evaluation of the absence of displacement of the soil strata along growth fault D are described in Part A of this response. Part B of this response describes the re-evaluation of the soil strata that was performed in order to determine the presence or absence of "caliche" (calcium carbonate) layers underlying the site and whether or not these caliche intervals can be used to constrain the timing of deformation of growth fault D.

Part A

The locations of the cross sections (X-X', Y-Y', W-W', and Z-Z') and profiles (E, F, and G) are shown in Figure 1. The explanation of the lithologies in the cross sections and profiles is shown as a legend in Figure 2. Cross sections X-X' and Y-Y' (Figures 3 and 4) were developed from the cross sections shown in SSAR Figures 2.5.1-34 and -35 while profiles E, F, and G (Figures 7, 8, and 9) were developed from the profiles shown in SSAR Figures 2.5.4-14, -15, and -16. Cross sections W-W' and Z-Z' (Figures 5 and 6) are new cross sections. With the exception of cross section X-X', all of the cross sections and profiles show the detailed stratigraphy beneath the site,

the projection of growth fault D (shown as GM-D) and its interpreted potential zone of deformation, and the LiDAR-derived topography. Cross section X-X' shows the detailed stratigraphy underlying the site in the Power Block Area.

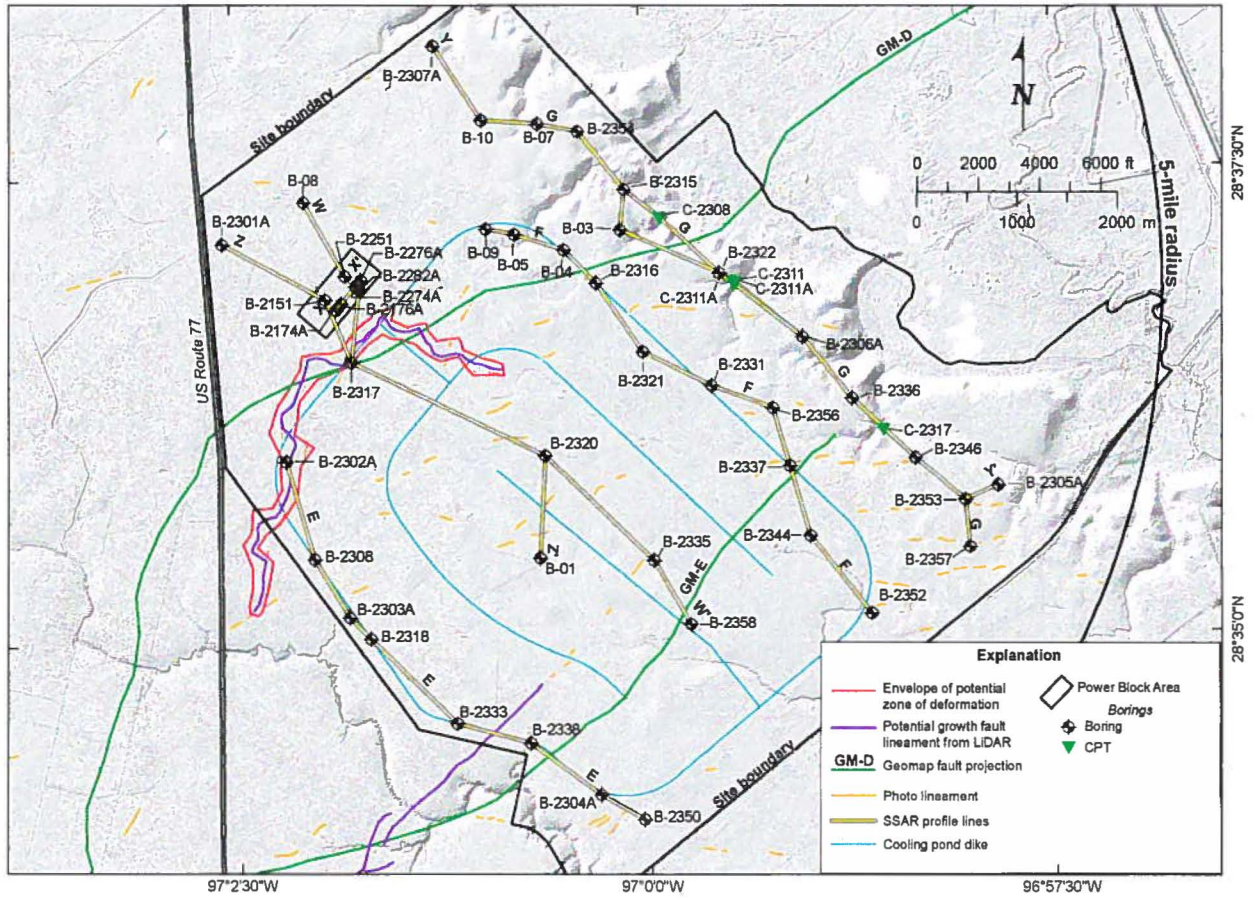
The LiDAR-derived topography data shown on the cross sections and profiles described above does not suggest that there is displacement or offset of the shallow soil strata underlying the site. That is, there appears to be no correlation between surface topography and irregular soil strata contacts. The gentle topographic slope between borings B-2302A and B-2303A shown in Profile E in Figure 7 appears to reflect the slope of the surface of the Beaumont Formation. The Sand 1/Clay 1-B contact is interpreted to be a distributary channel centered along boring B-2308 and flanked by overbank deposits and clay flats. This interpretation is preferred to a fault offset because the down-to-the-south sense of displacement is contradicted by the rise in the underlying Clay 1-B/Sand 2 contact. Cross sections W-W' and Z-Z' shown in Figures 5 and 6, respectively, also show gently dipping strata in the envelope of the potential zone of deformation, inferred to be distributary channel or overbank deposits, while the remaining cross sections and profiles generally show planar soil strata.

Part B

SSAR Subsection 2.5.1.2.3 contains descriptions of caliche intervals that are interpreted as a series of paleosols or time-stratigraphic marker beds. These caliche intervals are shown as dashed lines in the original cross sections X-X' and Y-Y' shown in SSAR Figures 2.5.1-34 and -35.

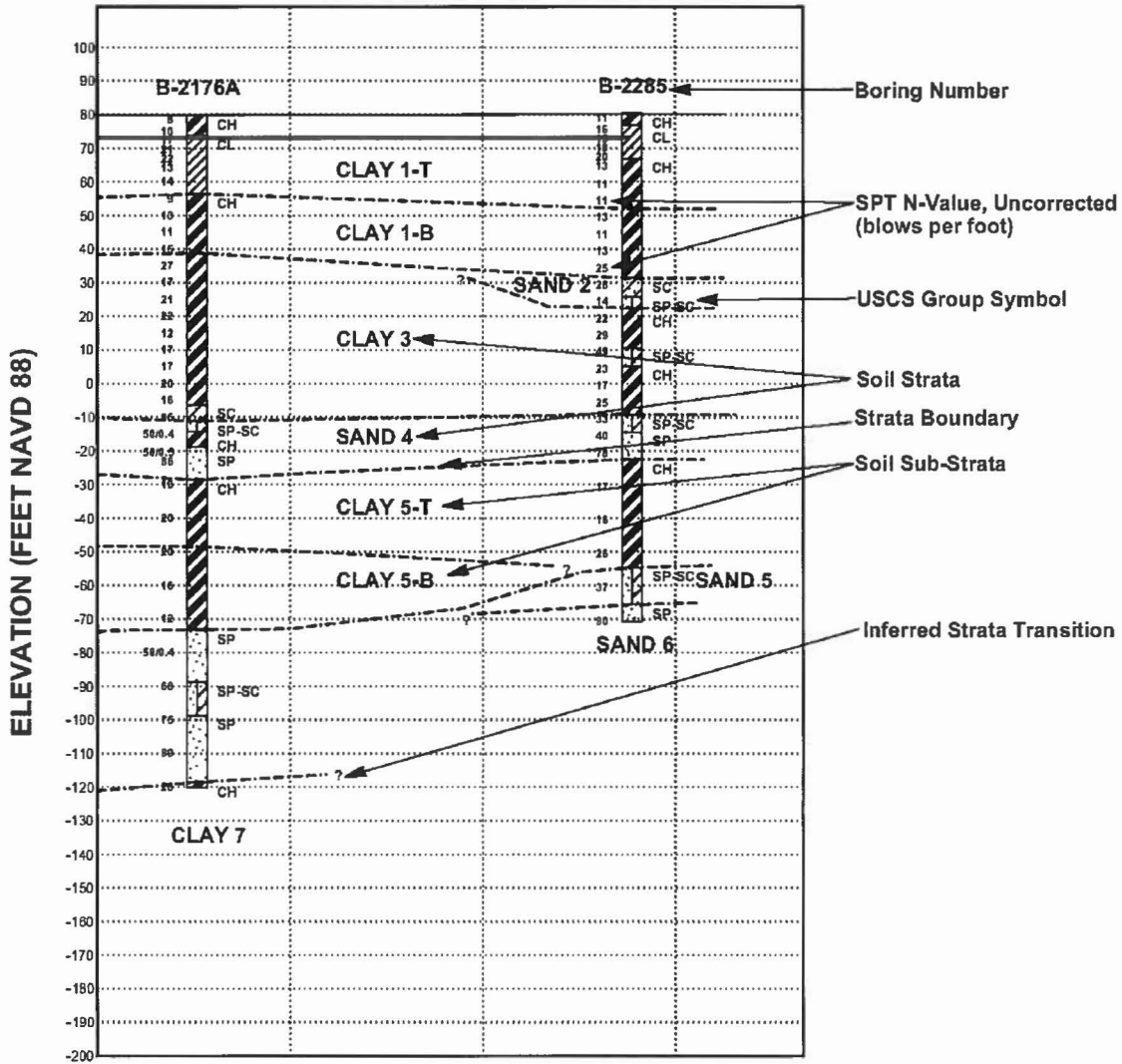
To verify their existence and provide more detailed descriptions of these caliche layers, a thorough review of the boring data (References 1–3) was performed. The review consisted of looking at field and final boring logs and tabulating the characteristics of the calcic deposits as well as trying to determine a set of criteria that could be used to define consistently a given caliche deposit. This re-evaluation revealed that while some of the descriptions on the soil boring logs clearly describe calcium carbonate deposits that may be interpreted as caliche, other descriptions are “trace carbonate nodule,” “few carbonate nodules,” “some carbonate nodules,” and “carbonate nodules” (References 1–3). Also, the calcic soils occur at various depths and cannot be correlated between borings by consistent depth or elevation, soil type, or soil density (SPT N values).

Based on this review, it is generally inferred that these calcic deposits have formed at various locations and depths across the site in response to changing arid or semiarid environmental conditions related to groundwater infiltration, variations in the water table elevation, and the nature of the fluvial deltaic Beaumont Formation. While it may be permissible to interpret some of these deposits as caliche, the deposits do not appear to be laterally continuous paleosols that can be correlated across the site or used as time-stratigraphic markers to constrain the timing of deformation along growth fault D. Therefore, the calcic deposits cannot be used to detect the presence or absence of subtle deformation patterns that might indicate potential off-set along growth fault D. A description of the currently preferred alternate interpretation will be added to a future revision to the ESPA, as described on page 12.



Note: Cross Section X-X' is within the Power Block Area and does not cross growth fault D (GM-D) or the envelope of potential zone of deformation.

Figure 1. Location of Cross Sections and Profiles

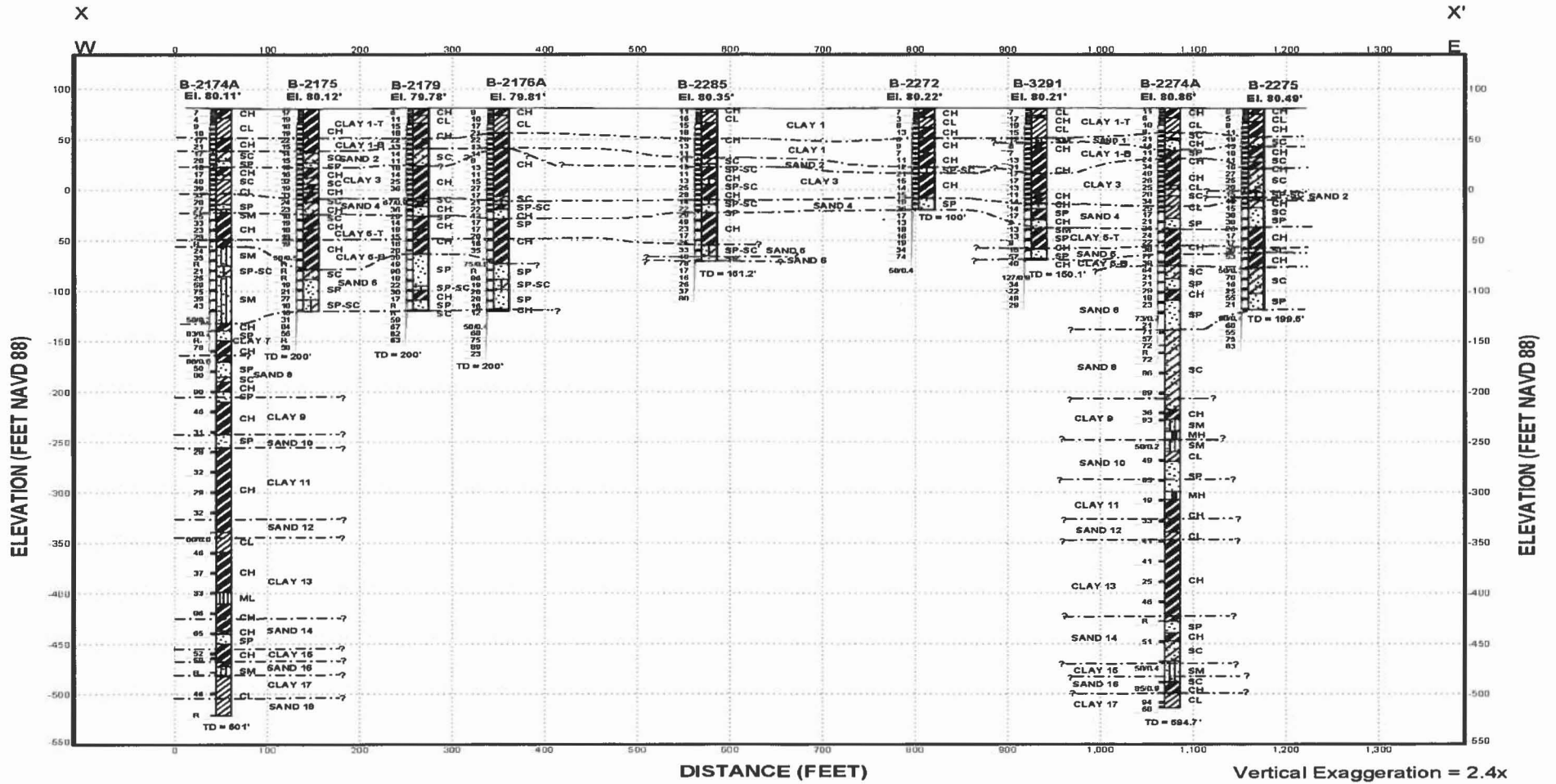


Notes:

- [1] See SSAR Section 2.5.4.2.1.2 text for stratum descriptions
- [2] Subsurface data have been obtained only at actual boring and CPT locations. Stratification shown between boring is based on extrapolation of the data obtained from the borings. Actual stratification between borings may differ from that shown.
- [3] In very hard soils, driving was terminated after 50 blows were recorded for a six-inch, or less, interval and the actual penetration recorded (e.g., 50 blows/0.3 feet).
- [4] The LiDAR elevation data are shown on cross sections Y-Y', W-W' and Z-Z' and profiles E, F and G (Figures 4 through 9) as a solid green line.

Adapted from SSAR Figure 2.5.4-3

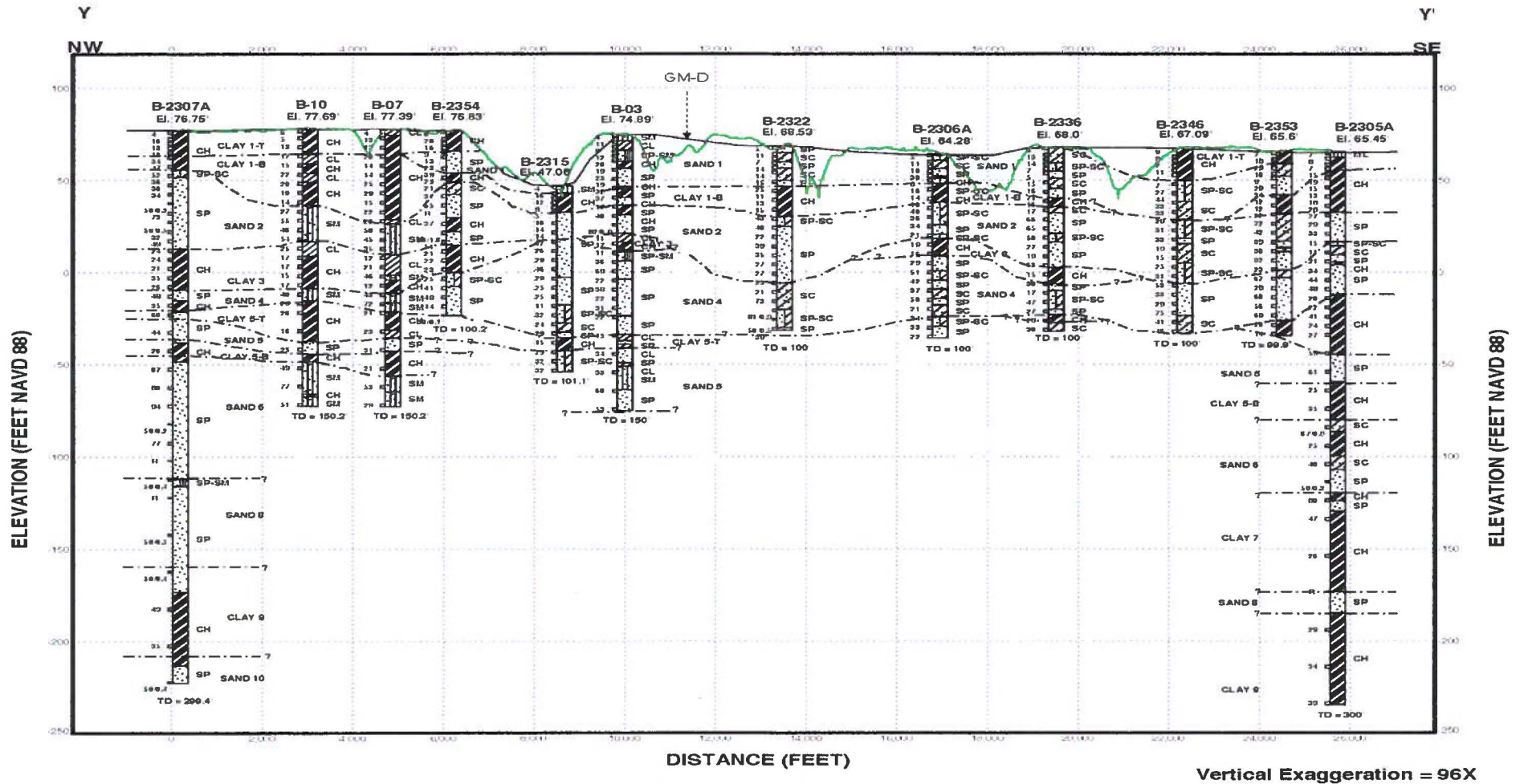
Figure 2. Cross Section and Profile Legend (Power Block and Cooling Basin Areas)



Note: For borings B-2175, B-2179, B-2176A, B-2285, B-2272, B-3291 and B-2275 the SPT N values are shown to extend below the bottom of the boreholes due to the vertical scale limitations.

Source: SSAR and Reference 1

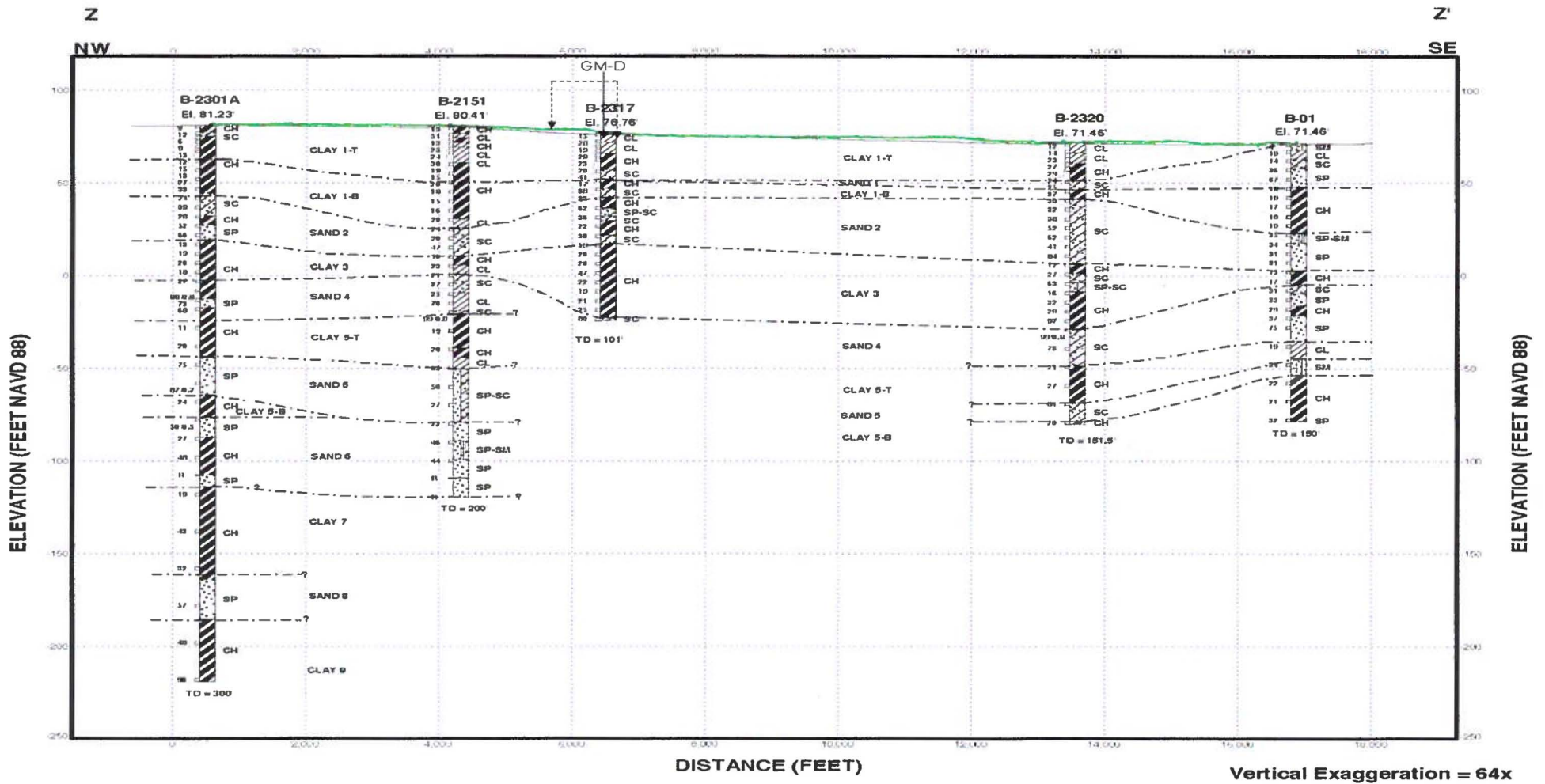
Figure 3. X-X' Cross Section



Note: For boring B-2353 USCS soil symbols have been omitted due to the horizontal scale limitations (see boring log B-2353 in Reference 3 for details). The dashed arrow is the approximate location of the Geomap (GM) fault D projection. See Figure 1 for location of Geomap fault D projection (GM-D). The green line is the LiDAR ground surface.

Source: SSAR and References 2 and 3

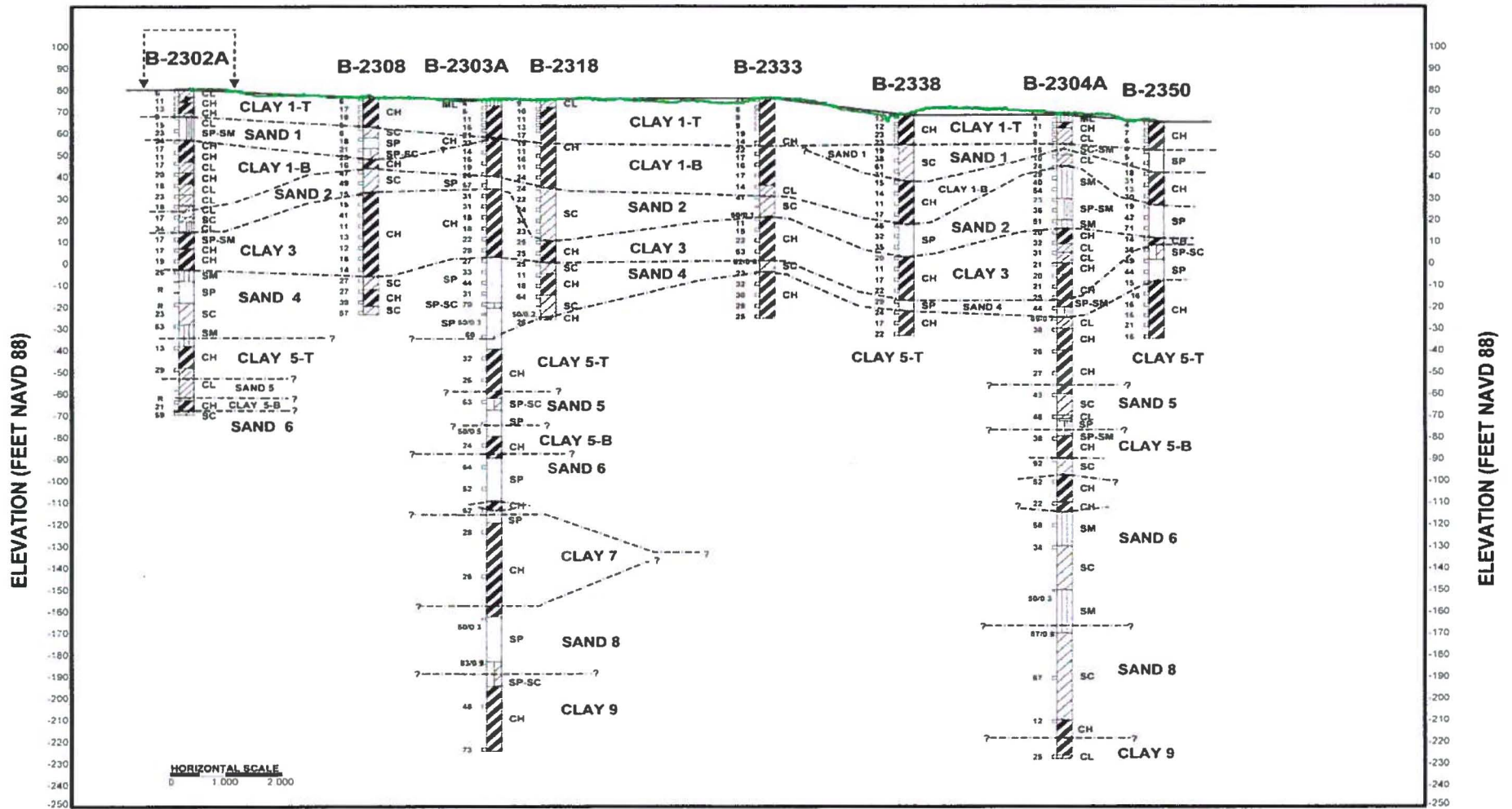
Figure 4. Y-Y' Cross Section



Note: The dashed line with arrows above the ground surface indicates the approximate location of the envelope of the potential zone of deformation of growth fault D. The solid arrow is the approximate location of the Geomap fault D projection (GM-D). The green line is the LiDAR-derived ground surface.

Source: SSAR and References 1, 2 and 3

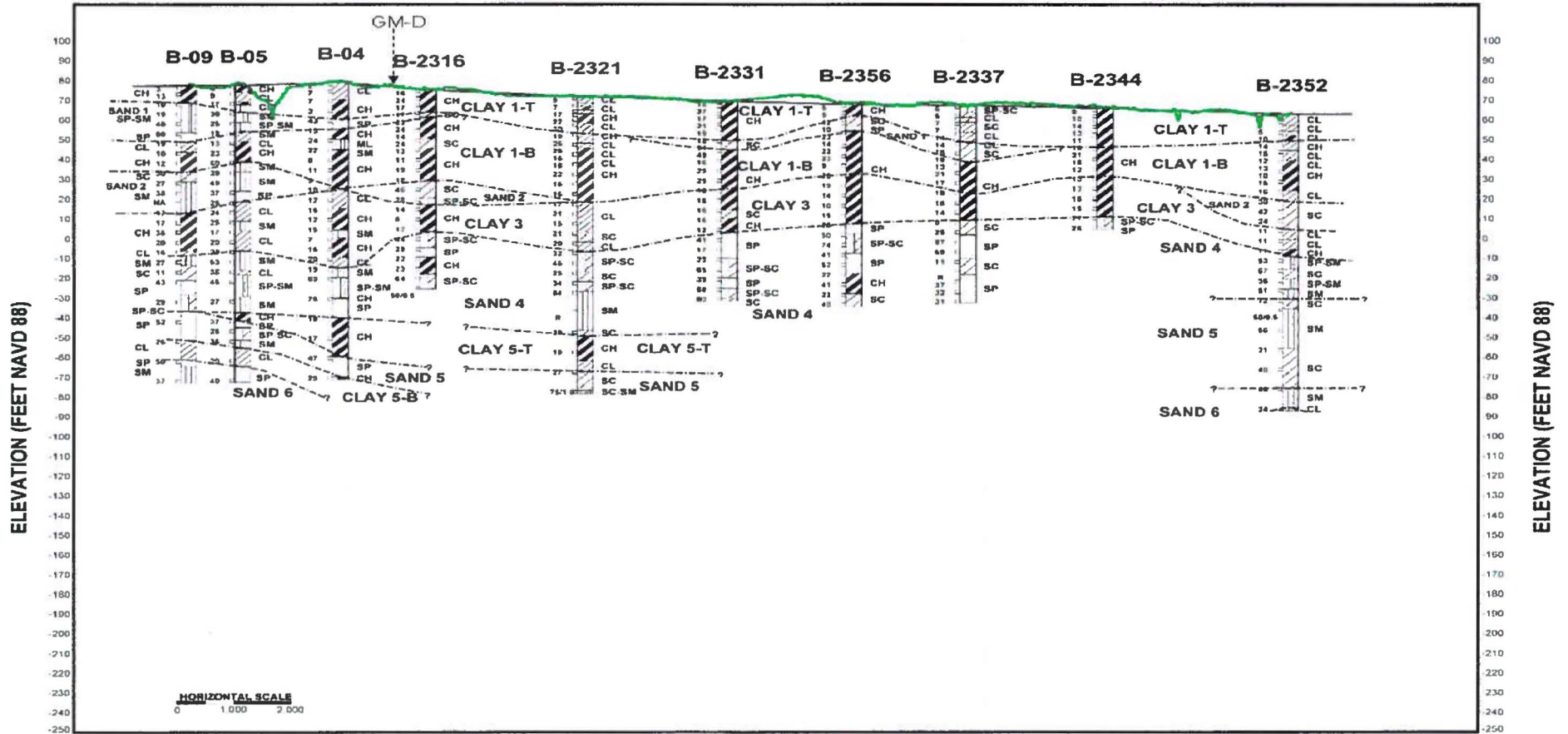
Figure 6. Z-Z' Cross Section



Note: The dashed line with arrows above the ground surface indicates the approximate location of the envelope of the potential zone of deformation of growth fault D. The green line is the LiDAR-derived ground surface.

Source: SSAR and References 2 and 3

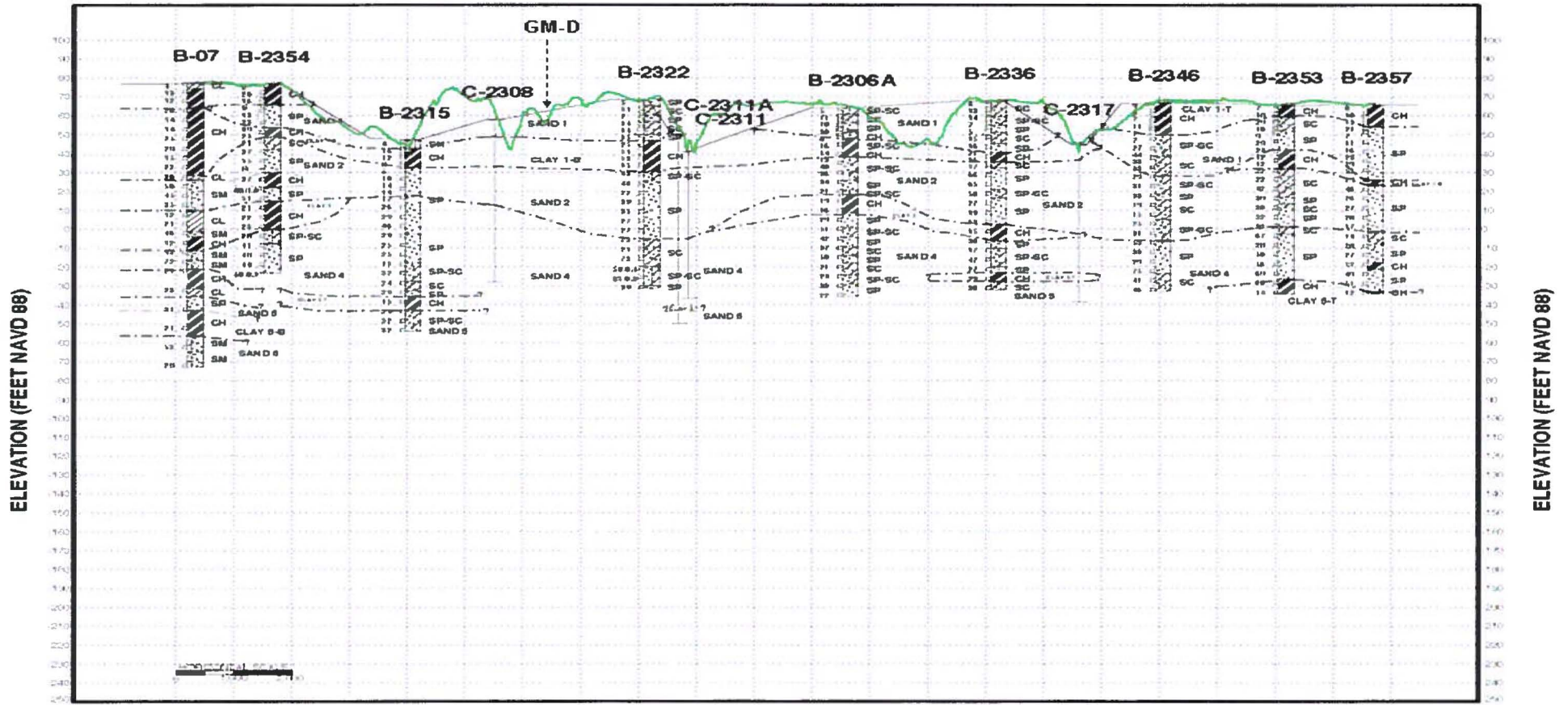
Figure 7. Profile E



Note: The dashed arrow is the approximate location of the Geomap (GM) fault D projection. See Figure 1 for location of Geomap fault D projection (GM-D). The green line is the LiDAR ground surface.

Source: SSAR and References 2 and 3

Figure 8. Profile F



Note: The dashed arrow is the approximate location of the Geomap (GM) fault D projection. See Figure 1 for location of Geomap fault D projection (GM-D). The green line is the LiDAR ground surface.

Source: SSAR and References 2 and 3

Figure 9. Profile G

Response Reference:

1. MACTEC Engineering and Consulting, Inc. (2008a). "Final Data Report, Geotechnical Exploration and Testing, Power Block, Exelon Texas COL Project, Victoria County Site," No. 25352-102-V14-CY00-00027-002 and 25352-102-V14-CY00-00029-003, Raleigh, NC.
2. MACTEC Engineering and Consulting, Inc. (2008b). "Final Data Report, Geotechnical Exploration and Testing, Cooling Basin, Exelon Texas COL Project, Victoria County Site," No. 25352-102-V14-CY00-00032-003 and 25352-102-V14-CY00-00034-003, Raleigh, NC.
3. MACTEC Engineering and Consulting, Inc. (2009). "Final Data Report, Geotechnical Exploration and Testing, Supplemental Investigation, Including UHS, Exelon Texas COL Project, Victoria County Site," No. 25352-102-V14-CY00-00044-002, Raleigh, NC.

Associated ESPA Revision:

The next-to-the-last paragraph of SSAR Subsection 2.5.1.2.3 will be revised in a future update of the ESPA as follows:

"Caliche" (calcium carbonate) occurs at several depths (Figures 2.5.1-34 and 2.5.1-35) across the VCS site. and since these These layers ~~represent~~ were originally interpreted as a series of ~~paleosoils, they are~~ paleosols that could be surmised as time-stratigraphic markers across the site. ~~In particular, the drilling in the power block area identified a caliche interval consistently at approximately 100 feet (30 meters) bgs.~~ A re-examination of the subsurface investigation data indicates that the preferred interpretation of calcium carbonate deposits in the Beaumont Formation is that they are ubiquitous and occur at various depths across the site. However, the available data indicate that correlations of these deposits among borings across the VCS site cannot be made with confidence. Uncertainties regarding this interpretation were expressed by showing interpretive correlations of the caliche layers as dashed lines on the cross sections cited above. Due to these uncertainties, caliche or calcic deposits are not a suitable means of constraining the timing of deformation along growth fault D.

RAI 02.05.01-12:**Question:**

In SSAR Sections 2.5.1.2.4.2.3.3 and 2.5.1.2.4.2.4 you presented slip rate calculations for faults D and E. In addition, in response to Question 02.05.01-01, ML 102510229, 8/16/2010, you stated that growth Fault E experienced movement during the Holocene (from 10,000 years before present up to today) and that growth Fault E is a short splay of Growth Fault D. Based on this structural relationship and the similarity in their surface expressions of deformation, you postulate that “post-Beaumont surface deformation could have occurred contemporaneously on both structures.” This implies that movement on Fault D cannot be limited to Beaumont age (100,000 yr) and may be more recent. However, this is the age you used in your calculation for the age and rate of movement on fault D, implying that it is not active.

In support of 10 CFR 100.23, please provide the following:

1. Present and compare topographic profiles of the fault E lineament in Beaumont, Holocene, and historic-aged deposits that document along-strike variations in fault topographic profile size and morphology. Discuss the implications of these comparisons for the age of initiation of fault E.
2. Discuss evidence for historical activity on faults D and E in light of recent public report that indicates growth fault E offsets pavement 8 inches on McFaddin Rd where the LiDAR lineament crosses this roadway.
3. Provide a re-evaluation of the rate of movement on fault D in light of these concerns and observations.
4. Compare these rates to published rates from other active growth faults in the region such as those in the Houston area.

Response:

This RAI response provides a detailed discussion of slip rate calculations for growth faults D and E. Each of the four requests in the RAI is addressed separately below. It is important to note that the vertical separation rates for the growth faults D and E are not relevant to the hazard at the VCS site because: 1) growth fault E is 2.6 miles south of the site, and therefore does not present surface faulting hazard to the VCS site (SSAR Figure 2.5.1-40); and 2) it is expected that the potential surface deformation associated with fault D will be contained within the zone of interpreted surface deformation (SSAR Figure 2.5.1-43). Therefore, regardless of the vertical separation rate across growth faults D and E there is no potential for these faults to produce surface deformation that could impact safety-related structures, systems, and components within the power block area (for further discussion see response to RAI 02.05.01-10).

1. The above RAI requests topographic profiles across the growth fault E where the topographic LiDAR lineament is mapped across Beaumont Formation, Holocene, and Historic deposits to document the along-strike variations in the lineaments morphology.

Figures 1 through 3 illustrate seven topographic profiles across growth fault E that crosses historic fill along FM Road 445 (called McFaddin Road in the RAI above), Holocene deposits, and Pleistocene deposits. Figure 1 shows the map view of the LiDAR lineament associated growth fault E and location of each topographic profile (including stationing along each profile). Figure 2 illustrates three profiles (G, H, and E1) across the LiDAR lineament where it is mapped across the Holocene San Antonio River floodplain (~10,000 year old; see response to RAI 02.05.01-1 for further discussion). Figure 3 illustrates one profile (V) across the FM Road 445 in artificial fill deposits (<100 yrs old) and three profiles (X, E2, and E3) in the Beaumont Formation deposits ($\geq 100,000$ years old) (See SSAR Subsections 2.5.1.2.3. and 2.5.1.2.4.2.3.3 for more details). Profiles E1, E2, and E3 are reproductions from Figure 2 in the response to RAI 02.05.01-11. Profile V was chosen because it is located in the middle of the FM Road 445. The other profiles shown in Figures 2 and 3 were chosen because they represented a subsample of topographic profiles where the LiDAR lineament associated with growth fault E is well-expressed topographically. For example, the LiDAR lineament crosses a small drainage between profiles E2 and E3 and splits into three different splays. Topographic profiles across this area do not show a well-resolved lineament, and therefore are not useful in a discussion of the age of initiation of growth fault E.

Figures 2 and 3 illustrate the extent of the growth fault E LiDAR lineament and Table 1 reports the height, width of the deformation zone, and age of the geologic deposits crossed by the lineament. Profiles G, H, and E1 document that the LiDAR lineament in the Holocene San Antonio River flood plain is between approximately 0.4 m to 1.3 m high and that the width of the deformation zone varies between approximately 20 to 55 m wide (Figure 2 and Table 1). Profile V documents the LiDAR lineament along the FM Road 445, which is approximately 0.3 to 0.75 m high and 20 to 40 m wide (Figure 3 and Table 1). Profiles X, E2, and E3 illustrate that the LiDAR lineament in the Beaumont Formation is between approximately 0.3 and 0.7 m high and the width of the deformation zone varies between approximately 15 to 52 m wide (Figure 3 and Table 1). The height of the potential zone of deformation of growth fault E shown in Table 1 is consistent with the maximum vertical relief of 1.5 m (4.9 ft) across the zone of deformation as discussed in response to RAI 02.05.01-13 and in SSAR Subsection. 2.5.1.2.4.2.4.

Table 1. Topographic profiles across the topographic lineament associated with growth fault E

<u>LiDAR Topographic Profile</u>	<u>Height (m)</u>		<u>Width (m)</u>		<u>Height (ft)</u>		<u>Width (ft)</u>		<u>Geologic Deposit</u>	<u>Deposits age (years)</u>
	Min	Max	Min	Max	Min	Max	Min	Max		
Profile V	0.3	0.75	20	40	0.98	2.46	66	131	Artificial Fill	<100
Profile G	0.4	0.75	53	55	1.31	2.46	174	180	Holocene	~10,000
Profile H	0.4	1.3	38	42	1.31	4.27	125	138	Holocene	~10,000
Profile E1	0.5	0.6	20	50	1.64	1.97	66	164	Holocene	~10,000
Profile X	0.4	0.45	25	35	1.31	1.48	82	115	Beaumont Formation	~100,000
Profile E2	0.4	0.7	42	52	1.31	2.30	138	171	Beaumont Formation	~100,000
Profile E3	0.3	0.4	15	40	0.98	1.31	49	131	Beaumont Formation	~100,000

These profiles do not indicate that the vertical separation across the topographic lineament associated with growth fault E has occurred since the construction of the FM Road 445, but more likely that the road was constructed across the pre-existing topographic break corresponding to the LiDAR lineament. There is a change in the topographic profile along the road where it is crossed by the LiDAR lineament (Figure 3), but field reconnaissance determined there is no obvious deformation of the road bed or pavement. If this vertical separation occurred since the construction of the road, it is likely there would be obvious signs of road distress. Given the subtle change in slope ($<1^\circ$) and broad nature of the potential zone of deformation associated with growth fault E, the road could have been constructed across the topographic anomaly with little or no grading of the original ground surface. Furthermore, where the growth fault E LiDAR lineament crosses the US Route 77 there is no topographic anomaly in the LiDAR data, which suggests that the vertical separation shown in Table 1 did not occur only in the last 100 years and that the FM Road 445 was constructed across a pre-existing lineament with minimal grading.

Based on the similarity in the height of the zone of potential deformation associated with the growth fault E topographic lineament between the historic artificial fill along the FM Road 445, Holocene deposits and the Pleistocene Beaumont Formation, it appears as though the age of initiation of the zone of deformation associated with growth fault E was after the deposition of the San Antonio River Flood plain or post-Holocene (10,000 year ago or less). As discussed in the response to RAI 02.05.01-13, this interpretation is consistent with a lower-bound Holocene vertical separation rate of approximately 0.0059 in/yr for the growth fault E LiDAR lineament.

The age of initiation of ground deformation associated with growth fault E of $\leq 10,000$ years does not necessarily indicate that the vertical separation rate of growth fault D should be revised because there is no evidence (except a weak association with growth fault E) that growth fault D offsets Holocene deposits.

2. The above RAI requests a discussion of the evidence (or data) presented in a recent public report, which states that fault E offsets the pavement 8 inches on McFaddin Road where the LiDAR lineament crosses the road.

The “recent public report” discussed in the above RAI refers to contentions to the VCS ESPA posed by a group named ‘Texans for a Sound Energy Policy’ (or TSEP), which hired John C. Halepaska and Associates, Inc. (John C. Halepaska and Associates, 2011; herein referred to as JCHA, 2011) to evaluate the VCS ESPA. The JCHA (2011) report is presented as Exhibit D-2 in the TSEP contention. Within the JCHA (2011) report, there are several assertions regarding the historical activity of faults D and E, including:

- Based on a comparison between 1970 and 2009 survey data where fault E crosses FM Road 445 (referred to above as McFaddin Road), JCHA (2011) claim “a dip of approximately eight inches or 0.67 feet” has occurred since the construction of the road and “the resulting movement rate of this growth fault [E] would be 0.2 inches per year, which is approximately 1,000 times larger than the rates estimated in the SSAR (0.00005-0.0005 in/yr)” (p. 110).

- Using cesium-137 age dating, the JCHA (2011) report states that “JCHA contracted Geo-hydro, Inc. (GHI) to take samples of depths varying from 0-56 cm from each side of “Growth Fault E” near where it crosses the San Antonio River. Results of analysis of these samples show an offset of at least 13 inches since the test era (c. 1960). This could suggest a rate of movement of 0.265 in/year, which is comparable to the estimate derived from the road survey above.” (p. 112).
- “JCHA collected samples from 4 boreholes spaced 75 feet apart straddling the anticipated trace of growth fault A near where it crossed the southern property boundary. The borings were drilled to a depth of 8 feet. Samples were collected at 3 inch intervals from the continuous cores and submitted for analysis of cesium-137[sic]. The results were consistent with possible recent movement of 7 inches across this fault.” (p. 112).
- “JCHA contracted GHI to observe the excavation of a series of trenches just North of the San Antonio River in the vicinity of the VCS Site (2008, Geo-Hydro, Inc.). These trenches showed a visible offset in near surface stratigraphy of at least 6 inches (Figure 4). Although dating of the offset was not performed, this corroborates that there has been movement across faults in the VCS area.” (p. 112).
- JCHA also reports contacting Union Pacific Railroad (UPR) to inquire about growth faults causing maintenance problems. UPR was not aware of the presence of growth faults in the area but reported that they “did observe a substantial amount of differential settling when working on the bridge over the San Antonio River located about four miles South of FM 445 along US Route 77” (p. 113).

Each of these bullets and the data presented by JCHA to support these conclusions are discussed below.

The existence of an eight-inch dip in FM 445 where growth fault E crosses the road is poorly constrained and associating the dip in the road to movement on the growth fault is speculative. First, the survey data presented in Figure 3 of the JCHA (2011) report have numerous features that bring into question the quality of the survey data. For example, there is a systematic offset between the 1970 and 2009 survey suggesting that there has been an overall uplift of the road along the entire length of the survey line since 1970, which is not discussed as a source of possible error. Second, there is a gap in the 1970 survey data at the location of the growth fault. The report does not explain how eight inches of deformation were measured given this data gap, thus making the claim of post-1970 deformation difficult to support. Third, there are numerous anomalies within the survey data on the same order of magnitude as the 8-inch dip that are not accounted for or discussed in JCHA (2011), suggesting that there may be factors unrelated to growth faults causing the purported changes in the road elevation with time. Attributing the 8-inch dip to growth fault movement is speculative because the JCHA (2011) report provides no evidence that supports the hypothesis that the dip is related to the growth fault. For example, the report does not present any seismic reflection data or trench data from the road to demonstrate that the dip is directly related to subsurface faulting.

Regarding the JCHA (2011) report of post-1960's offset in near surface stratigraphy and in shallow boreholes inferred from using Cesium-137 data, these conclusions are difficult

to evaluate based on the lack of data presented in the JCHA (2011) report. First, the general standard of practice for conducting paleoseismic studies of active faults includes providing a description of the locations of the samples, and documenting subsurface evidence of suspected faults through maps, boring logs, trench logs, sample depth information, testing results (including laboratory and calibration information) and photographs (McCalpin, 2009). Without this information there is no way to independently evaluate the quality/validity of these claims. In addition, a difference in Cesium-137 concentrations at depth is not clear evidence of fault movement. An alternative explanation for differences in Cesium-137 concentrations across the growth fault is that flooding associated with the San Antonio River or possibly anthropogenic activities reworked soil at the sample site and disturbed the original stratigraphy. The standard of practice methodology to rigorously test this hypothesis is to clearly document the stratigraphy at the site to demonstrate the absence of fluvial reworking and the presence of the original soil stratigraphy. The JCHA report (2011) does not provide any such documentation, and thus attributing differences in Cesium-137 concentration to growth fault movement is unsupported and speculative.

Regarding the trenches excavated north of the San Antonio River in the vicinity of the VCS Site reported by JCHA (2011), there are very little data presented to support the claims/conclusions that the near surface stratigraphy has been visibly offset, and therefore these claims are difficult to evaluate. Again, the standard of practice methodology used to document offset stratigraphy in a trench (e.g. McCalpin et al., 2009) requires the detailed logging and description of the trench exposure (i.e., creating a detailed, continuous map of the trench exposures based on field observations, photographs, and descriptions of the shallow stratigraphy and soil). In contrast, the contention that near-surface stratigraphy is offset (Figure 4 of JCHA [2011] report) is based on five discrete data points taken over 55 feet. With such sparse discontinuous data, it is impossible to accurately characterize features present within the trench (i.e., offset horizons) or hypothesize what may have caused them. Evidence of problems developing conclusions from such sparse data and non-continuous observations can be seen in the data where the elevations at distances of 0 and 55 feet for both layer interfaces are essentially the same, suggesting that there is no net offset across the fault over 50 feet. The JCHA (2011) report provides no discussion or description of the material excavated making it impossible to independently evaluate the quality of these observations. For example, it is not possible to determine whether JCHA mapped an actual fault offset, or if this offset is simply inferred (contrary to the interpretation of seismic reflection data and topographic data presented in the VCS ESPA, which document broad-scale folding rather than faulting). Therefore, it is impossible to understand, evaluate, and review these claims of recent surface deformation associated with the growth fault E LiDAR lineament in a way that provides a meaningful comparison to the topographic data presented in part 1) of this response and the VCS ESPA.

Regarding the settlement that occurred during work on a bridge over the San Antonio River, there are many well-documented non-tectonic mechanisms of differential settlement that are not associated with growth faults. UPR did not conduct a detailed site-specific investigation to determine the cause of the settlement, and there are no compelling data in the JCHA (2011) report that provides a spatial association with a potential growth fault and the bridge in question. Thus, this report of settlement has not been shown to be associated with the historic activity on growth faults D and E. Furthermore, JCHA (2011) did not systematically address all the possible settlement

mechanisms (other than growth faulting), and did not provide arguments why such mechanisms should be rejected in favor of a growth fault hypothesis.

In summary, it is not possible to perform critical review of the conclusions presented in the JCHA report (2011) without more detailed information, and proper documentation of the data. Therefore, Exelon is reluctant to use data from this report as evidence for historic activity on growth faults D and E. This position is supported by the overall approach of NUREG/CR-5562 (Sowers, et al., 1998). The NRC has sponsored the preparation of NUREG/CR-5562, which addresses the age-dating techniques used for paleoseismic investigations. NUREG/CR-5562 outlines the overall approach to such studies and provides recommendations/conclusions for these investigations at the end of this volume (Sowers, et al., 1998). An excerpt of these recommendations/conclusions is presented below:

- 1) "each method [used to date geologic deposits] has a very specific set of assumptions that must be satisfied for the method to be valid." (p. 5-12)
- 2) "Verification of the accuracy of age estimates should be made." (p. 5-14)
- 3) "Complete data should be reported according to standards set in the literature." (p. 5-14).
- 4) Error analysis should be rigorous and should account for all sources of uncertainty" (p. 5-14).

The JCHA report (2011) provides no description of the methodology used; no discussion of why the assumptions used as part of the Cesium-137 dating technique are valid; no description of the accuracy associated with any of the conclusions; there is very little detail in this report; and no discussion of possible sources of error or uncertainty.

3. Part 3 of this RAI requests a re-evaluation of the rate of movement on fault D based on the information described in the JCHA (2011) report.

As discussed in part 2 of this response, the limited data and discussion presented in the JCHA (2011) report makes providing a meaningful comparison to or update of the potential average vertical separation rate across growth fault D presented in the SSAR problematic and inappropriate. However, to be responsive to this RAI a comparison between the two rates is explored below. JCHA (2011) reports between six and 13 inches of post-1960's movement on growth fault E. These offsets infer a potential average historic (post-1960s) rate of vertical separation between 0.12 and 0.265 in/year.

The minimum vertical separation rate across the growth fault E topographic lineament is addressed in the response to RAI 02.05.01-13, which reports that a long-term average Holocene separation rate across the growth fault D LiDAR lineament of approximately 0.0059 in/per year (based on 4.9 ft divided by 10,000 years). This rate is based on an inferred maximum age of Holocene deposits of 10,000 years. There is no information available to provide additional constraints on rate based on younger deposits deformed by growth fault E, so the rate of 0.0059 in/yr must be regarded as a minimum average Holocene rate.

The difference between these two rates is large. However, the very limited nature and limited documentation of the JCHA (2011) study make a re-evaluation of the rate of movement on fault E inappropriate based on their conclusions. For example, the total offset of the late Pleistocene Beaumont surface is not provided at the sites described in

the JCHA (2011) report for comparison with the Historic surfaces, and there is no discussion of faulting of Holocene sedimentary deposits, other than the inferred offset of historic deposits. Thus, Exelon cannot provide a comparison between the long-term average rates presented in the SSAR and the higher historic vertical separation rates presented by the JCHA (2011) report.

4. Compare these rates to published rates from other active growth faults in the region such as those in the Houston area.

Published rates from the Houston area, where historic growth fault movement is well studied and has been linked to subsurface fluid withdrawal of hydrocarbon and groundwater resources, range from 0 to 1.2 in/yr (1 to 30 mm/yr) (Engelkemeir, et al., 2010; Engelkemeir, et al., 2006; Engelkemeir and Khan, 2008; Holzer and Gabrysch, 1987; Kreitler, 1978; Verbeek, et al., 1979). The active movement of faults and regional subsidence in the Houston area have been studied through campaign-style surveys (Holzer and Gabrysch, 1987; Mastronianni, 1991), geodetic studies (Engelkemeir, et al., 2010), and interferometry (Buckley, et al., 2003). High rates of growth fault creep are generally associated with areas of high subsurface fluid extraction, the movement of salt domes at depth, and sediment compaction.

The vertical separation rate of Houston-area growth faults and rates from the JCHA (2011) report are higher than the lower-bound estimate across the growth fault E LiDAR lineament near the VCS Site (0.0059 in/yr). However, these higher estimates do not indicate that the lower-bound separation rates across the growth fault E LiDAR lineament are incorrect. First, Houston area growth fault activity has been linked to subsurface fluid extraction (e.g. Holzer and Gabrysch, 1987). Per the response to RAI 02.05.01-14, a similar statement cannot be made to growth faults in the VCS Site Area because 1) high historic rates of growth fault movement has not been documented in the VCS Site Area and 2) there are no studies or data in the VCS Site Area that relate subsurface fluid extraction to growth fault activity. Thus, invoking Houston area growth fault activity as a possible analog to the VCS site is inappropriate. Second, field reconnaissance performed as part of this ESPA identified no compelling evidence for historic growth fault deformation along growth fault E, in contrast to well-documented historic and active growth fault movement in the Houston area. Third, the discussion presented in part 2) of this response provides a detailed explanation of why the data and conclusions presented in the JCHA (2011) report appear poorly constrained and should not be used to assess recent growth fault activity at the VCS site. Thus, there are no reliable data available to further assess vertical separation rate across the growth fault E LiDAR lineament at the VCS Site.

Regardless of the differences in rate discussed above, the vertical separation rates of the growth faults D and E LiDAR lineaments are not relevant to hazard at the VCS site because: 1) growth fault E is 2.6 miles south of the site and therefore, does not present a surface faulting hazard to the VCS site (SSAR Figure 2.5.1-41); and 2) it is expected that the potential surface deformation associated with fault D will be contained within the zone of interpreted surface deformation (SSAR Figure 2.5.1-43). Thus, there is no potential for these growth faults to produce surface deformation (i.e. folding) that could impact safety-related structures, systems, and components within the power block area and failure of the cooling basin above fault D would not adversely impact the safety of operation of the plant (for further discussion see response to RAI 02.05.01-10).

A future revision to the SSAR reflecting the above response is described on pages 12 - 13.

Response References:

Buckley, S. M., Rosen, P. A., Hensley, S. and Tapley, *Land subsidence in Houston, Texas, measured by radar interferometry and constrained by extensometers*: Journal of Geophysical Research, v. 108, p. 8-1 to 8-13, 2003.

Engelkemeir, R., Khan, S. and Burke, K., *Surface deformation in Houston, Texas using GPS*: Tectonophysics, p. 47-54, 2010.

Engelkemeir, R., Khan, S. and Norman, C., *Mapping active faults in the Houston area using LIDAR*, AAPG Annual Meeting, Houston, TX, 2006.

Engelkemeir, R. M. and Khan, S. D., *Lidar mapping of faults in Houston, Texas, USA*: Geosphere, v. 4, p. 170-182, 2008.

Holzer, T. and Gabrysch, R., *Effect of water-level recoveries on fault creep, Houston, Texas*: Ground Water, v. 25, p. 392-397, 1987.

John C. Halepaska and Associates, I., *Contest Issues Concerning Early Site Permit Exelon's Victoria County Station*: Littleton, CO, prepared for the Texans for a Sound Energy Policy, p. 162, 2011.

Kreitler, C. W., *Faulting and Land Subsidence from Ground-Water and Hydrocarbon Production, Houston-Galveston, Texas*: Austin, TX, Bureau of Economic Geology, Research Note 8, p. 22, 1978.

Mastronianni, J. J., *A Study of Active Fault Movement Houston, Texas and Vicinity* [Masters thesis]: Houston, University of Houston, p. 150 1991.

McCalpin, J. P., *Paleoseismology, Second Edition*, Academic Press, 2009.

Sowers, J. M., Noller, J. S. and Lettis, W. R., *Dating and Earthquakes: Review of Quaternary Geochronology and Its Application to Paleoseismology (NUREG/CR-5562)*: Washington DC, US NRC, 1998.

Verbeek, E. R., Ratzlaff, K. W. and Clanton, U. S., *Faults in Parts of North-Central and Western Houston Metropolitan Area, Texas*: Reston, VA, US Geological Survey, Miscellaneous Field Studies Map 1136, 1979.

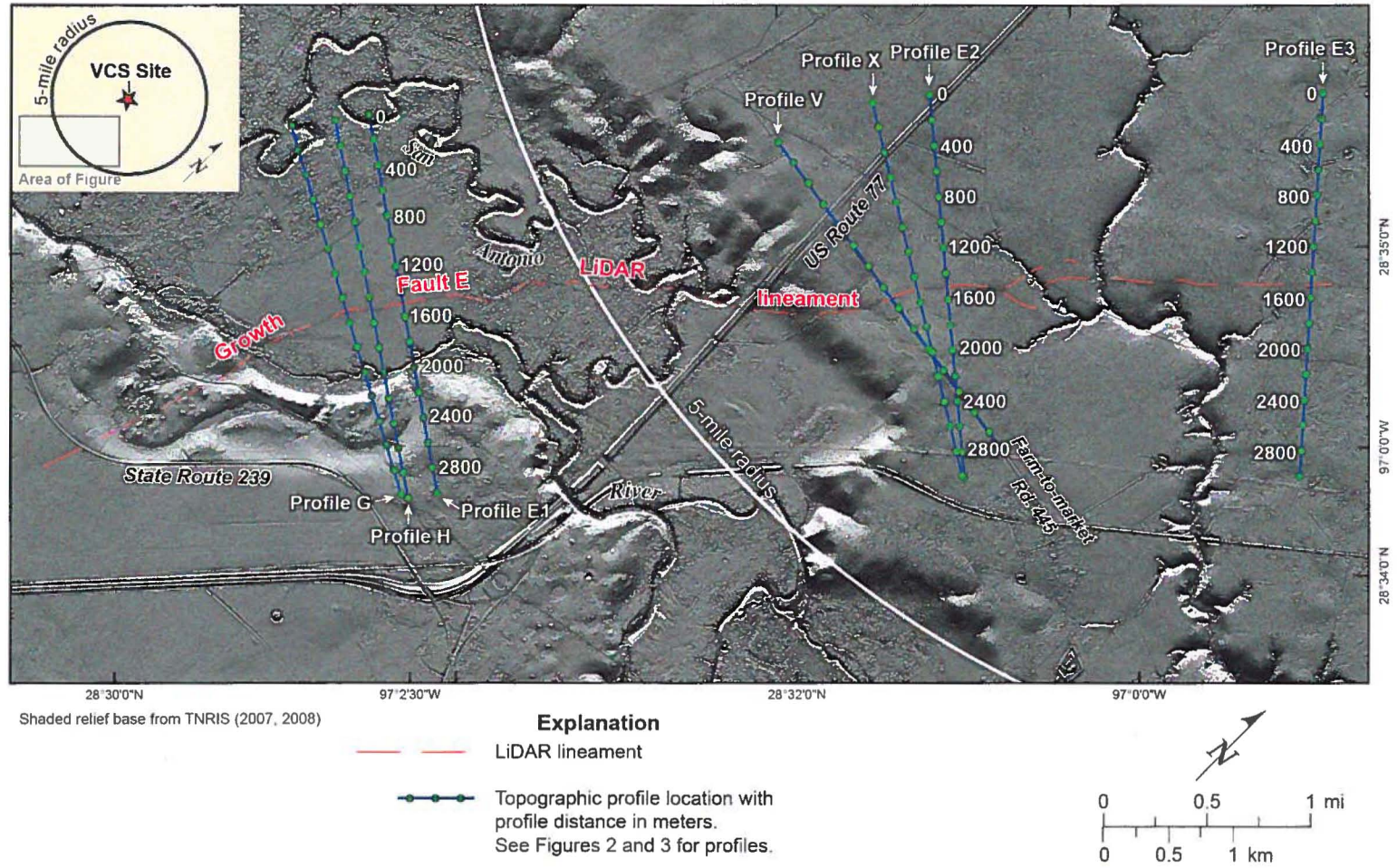
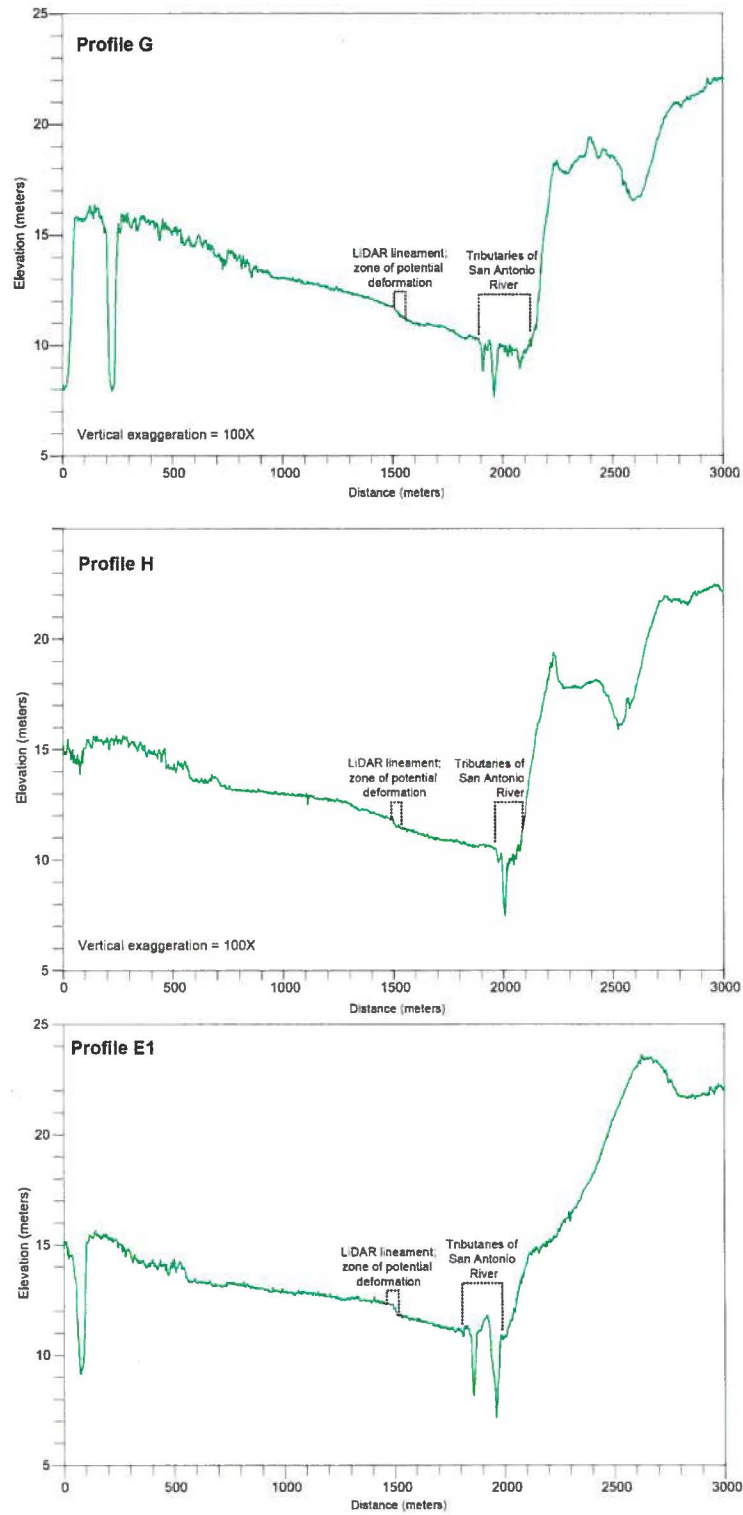


Figure 1. Location of Fault E LiDAR Profiles.



See Figure 1 for profile locations

Figure 2. Topographic Profiles E1, G, and H across Growth Fault E in Holocene Deposits.

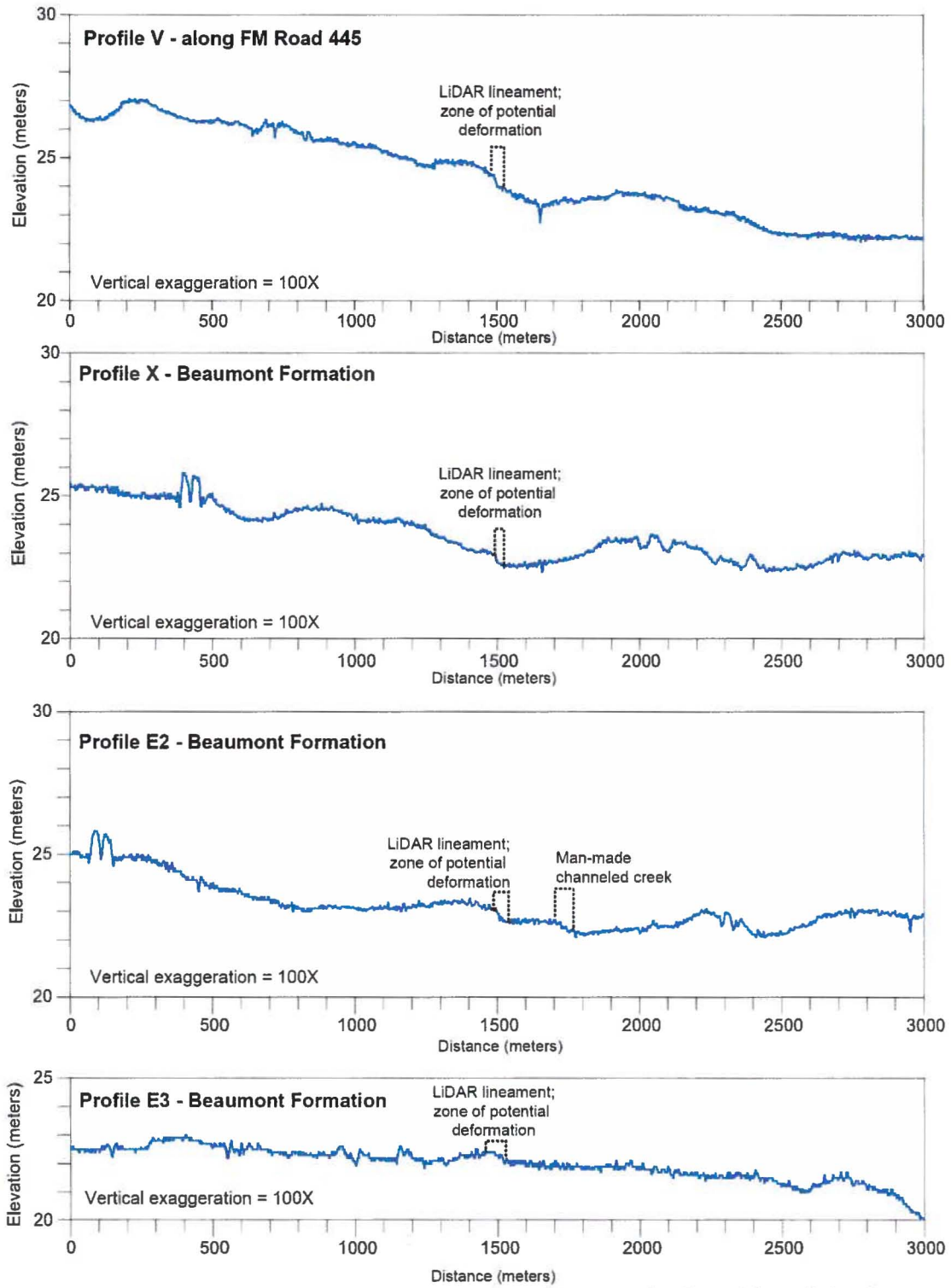


Figure 3. Topographic Profiles V, X, E2, and E3 across Growth Fault E.

Associated ESPA Revision:

As a result of the response to RAI 02.05.01-1, the site area geological map (SSAR Figure 2.5.1-4) was revised. As a result, revisions to SSAR Section 2.5.3 are provided below.

The third paragraph of SSAR Subsection 2.5.3.4.2.1 shall be revised in a future revision of the ESPA as follows:

Fault GM-E is not adequately imaged by reflection data to assess activity or non-activity since deposition of the Horizon 3 and Horizon 4 seismic markers. In lieu of direct seismic imaging, activity or non-activity of fault GM-E was assessed through geomorphic analysis. Subtle topography imaged by LiDAR data indicates that a distinctly linear, southeast-facing slope break associated with the updip projection of fault GM-E is present in the upper surface of the middle to late Pleistocene Beaumont Formation. The lineament can be traced to the southwest where it is present in relatively younger Holocene deposits and landforms of the San Antonio river valley (Figure 2.5.1-39; see Subsection 2.5.1.2.4.2.3). These relationships provide strong evidence that the lineament and associated southeast-facing slope break were not formed by fluvial processes, and that the lineament is clearly post-Beaumont in age where it crosses the Holocene San Antonio River valley deposits. Based on these observations, the lineament is interpreted to be associated with local Quaternary Holocene activity of growth fault GM-E.

The SSAR Subsection 2.5.3.4.2.1.2 shall be revised in a future revision of the ESPA as follows:

Growth fault GM-E is over 2.6 miles (4.2 km) from the power block area, and as such, any activity on the fault will not affect the site. Despite this fact, fault GM-E is still a structure of interest because it is the only fault, besides fault GM-D, that exhibits evidence for Quaternary activity within the site area. As described in Subsection 2.5.1.2.4.2.3.1.3, fault GM-E is not imaged in the seismic reflection data because the seismic profiles do not extend far enough south to cross the fault and provide sufficient imaging resolution of the fault at depth. Despite the lack of direct reflection imaging, the distinct topographic lineament apparent in the LiDAR data and its spatial correlation with the surface projection of fault GM-E strongly suggest that fault GM-E has been active in the Quaternary and formed a monoclinial, southeast-facing slope break in the upper surface of the Beaumont Formation, similar to that associated with fault GM-D.

As described in Subsection 2.5.1.2.4.2.4, fault GM-E crosses a variety of features including the deposits of the Beaumont Formation, younger Pleistocene Holocene stream terrace and floodplain deposits of the San Antonio River, and man-made features (i.e., FM 445, U.S. Highway 77, and SR 239) (Figures 2.5.1-4 and 2.5.1-39). Field reconnaissance of the fault across these features was unable to provide any refinements on the timing of activity other than that movement has occurred since deposition of the Beaumont Formation and younger Holocene sediments of the San Antonio river valley. Topographic profiles of the fault along FM 445 derived from the LiDAR data reveal that the slope break associated with the fault has the same characteristics as the non-eroded profiles of fault GM-D (e.g., Profiles 4 and 8 in Figures 2.5.1-50a and 2.5.1-50b, respectively): a distinct inflection of the ground surface at the location of the lineament with the southeast side down. For fault GM-E, this step has an approximately 4.9 feet

(1.5 meters) topographic offset over 980 feet (300 meters), or equivalently a narrow, steepened region with a slope of approximately 0.29 degrees.

The second paragraph of SSAR Subsection 2.5.3.4.2.1.3 shall be revised in a future revision of the ESPA as follows:

Using a similar approach, with topographic relief on the surface of the Beaumont Formation and the Holocene San Antonio River floodplain deposits determined from analysis of LiDAR profiles, the ~~range lower-bound Holocene in long-term~~ deformation rates for fault GM-E is ~~1.7×10^{-4} inches per year to~~ 5.9×10^{-3} inches per year. This vertical relief and implied range of deformation rates are similar to those observed for fault GM-D. The similarities between the two faults could either be coincidental or may suggest that the mechanisms, rates, and characteristics of growth fault activity within the site area are fairly uniform (see Subsection 2.5.1.2.4.2.4).

The second paragraph of SSAR Subsection 2.5.3.7 should be revised as follows:

Interpretation of aerial photography and LiDAR data, coupled with aerial and field reconnaissance, has documented Quaternary surface deformation associated with growth faults GM-D and GM-E in the site area (see Subsection 2.5.1.2.4.2.3). Detailed analysis of seismic reflection and LiDAR data indicate that displacement on faults GM-D and GM-E can be traced upwards to very shallow depths in the stratigraphic section. Displacement on these structures at depth projects updip to distinct lineaments in the LiDAR data that coincide with zones of mappable southeast-side-down monoclonal tilting of the upper depositional surface of the Quaternary Beaumont Formation and the Holocene San Antonio River flood plain deposits. The closest approach of a zone of monoclonal tilting the power block area is approximately 509 feet (155 meters) (Figure 2.5.1-43) (see Subsection 2.5.1.2.4.2.3.2). The extent of monoclonal surface deformation is discernable from analysis of LiDAR data, and does not require detailed investigations of the type used to characterize potential surface rupture on capable tectonic faults.

ATTACHMENT 3

SUMMARY OF REGULATORY COMMITMENTS

(Exelon Letter to USNRC, NP-11-0035, dated August 4, 2011)

The following table identifies commitments made in this document. (Any other actions discussed in the submittal represent intended or planned actions. They are described to the NRC for the NRC's information and are not regulatory commitments.)

COMMITMENT	COMMITTED DATE	COMMITMENT TYPE	
		ONE-TIME ACTION (Yes/No)	Programmatic (Yes/No)
Exelon will revise the VCS ESPA SSAR Section 2.5.1 to incorporate the change shown in the enclosed response to the following NRC RAI: 02.05.01-5 (Attachment 1)	Revision 1 of the ESPA SSAR and ER planned for no later than March 31, 2012	Yes	No
Exelon will revise the VCS ESPA SSAR Section 2.5.3 to incorporate the change shown in the enclosed response to the following NRC RAI: 02.05.01-12 (Attachment 2)	Revision 1 of the ESPA SSAR and ER planned for no later than March 31, 2012	Yes	No